Single particle detection: Phase control in submicron Hall sensors

Lorenzo Di Michele, Connor Shelly, John Gallop, and Olga Kazakova[a)]
National Physical Laboratory, Teddington TW11 0LW, United Kingdom

(Received 23 July 2010; accepted 13 October 2010; published online 30 November 2010)

We present a phase-sensitive ac-dc Hall magnetometry method which allows a clear and reliable separation of real and parasitic magnetic signals of a very small magnitude. High-sensitivity semiconductor-based Hall crosses are generally accepted as a preferential solution for non-invasive detection of superparamagnetic nanobeads used in molecular biology, nanomedicine, and nanochemistry. However, detection of such small beads is often hindered by inductive pick-up and other spurious signals. The present work demonstrates an unambiguous experimental route for detection of small magnetic moments and provides a simple theoretical background for it. The reliability of the method has been tested for a variety of InSb Hall sensors in the range 600 nm–5 μm. Complete characterization of empty devices, involving Hall coefficients and noise measurements, has been performed and detection of a single FePt bead with diameter of 140 nm and magnetic moment of $\mu \approx 10^8\ \mu_B$ has been achieved with a 600 nm-wide sensor. [doi:10.1063/1.3514097]

I. INTRODUCTION

Several experimental techniques, such as superconductor quantum interference device, giant magnetoresistance and Hall effect sensors have been adopted in the last few years for magnetic properties characterization of nanostructured materials. All these techniques have their own preferential applications depending on the optimal experimental conditions and sensitivity.

Micron and submicron sized semiconductor based Hall sensors are preferred for a number of biomedical, chemical and environmental applications because of their high sensitivity at room temperature and the non-invasive nature of the measurements.[1–3] The employment of such devices as a part of multi-purpose biosensors has been proposed with the aim of detecting single nanobeads used as magnetic biological labels.[4] Micron sized beads are already commercially available and single particle detection has been successfully carried out.[1,5–7] Nevertheless, the goal of single molecule labeling motivates a further reduction of bead dimensions and consequently the development of smaller and more sensitive sensors and safer and more reliable detection schemes.

Detection is usually carried out by applying both dc and ac magnetic fields to a sensor provided with a bead (or an empty sensor, in a control experiment) and measuring the ac Hall voltage. Variations in the ac Hall voltage in response to a step-wise dc field are generally accepted as evidence of the bead presence.[1–6,8,9]

While bead dimensions and momenta are reduced, signals generated by inductive couplings, foreign ferromagnetic materials in the vicinity of the device as well as low frequency, $1/f$, noise might mask true bead signals. Employing non-invasive, ultra-sensitive InSb Hall bars, this work aims to understand these artifact signals and develop an optimized measurement setup able to separate them from the proper bead signal allowing the detection of submicrometer beads. Taking as a reference the ac field phase, the possibility to separate inductive signals from those ascribable to the magnetic materials in the out-of-phase and in phase components, respectively, are demonstrated and both the ac frequency and dc amplitude are optimized. The detection of a single FePt bead ($\varnothing$ 140 nm, $\mu \approx 10^8\ \mu_B$) with this optimized setup is reported.

II. EXPERIMENTAL

Hall bars of widths between 600 nm and 5 μm were fabricated using e-beam lithography and reactive ion etching of 300 nm thick undoped InSb films grown by molecular beam epitaxy onto semi-insulating GaAs substrates. Further details on the fabrication procedure are provided in Ref. 6. The electron mobility $\mu_e = 1.3\ \mathrm{m^2/V\,s}$ and concentration $n \approx 3.9 \times 10^{16}\ \mathrm{cm^{-3}}$ were deduced by magnetoresistance measurements.

Ohmic electric contacts were formed by depositing titanium/gold layers. A first group of devices showed a high two-terminal resistance of $R_2 = 70–80\ \mathrm{k\Omega}$, mainly due to the high resistivity of InSb leads, and a lower four-terminal resistance $R_4 = 7–9\ \mathrm{k\Omega}$. A second group was provided with longer gold leads resulting in a two-terminal resistance of $R_2 = 5–15\ \mathrm{k\Omega}$ which is still, however, larger than the calculated one. This expedient allowed in many cases a significant reduction of the noise level which in this case is mainly ascribable to fluctuations in the resistance across voltage terminals.[10]

Each sample was constructed of two symmetric crosses connected via the current lead. When a particle was present on one of the crosses, the second one was left empty as a control device (Fig. 1).

In order to place a bead at the fixed position on the Hall cross and protect the material from elevated temperatures and radiation damage during the manipulation process, the

[a)]Electronic mail: olga.kazakova@npl.co.uk.

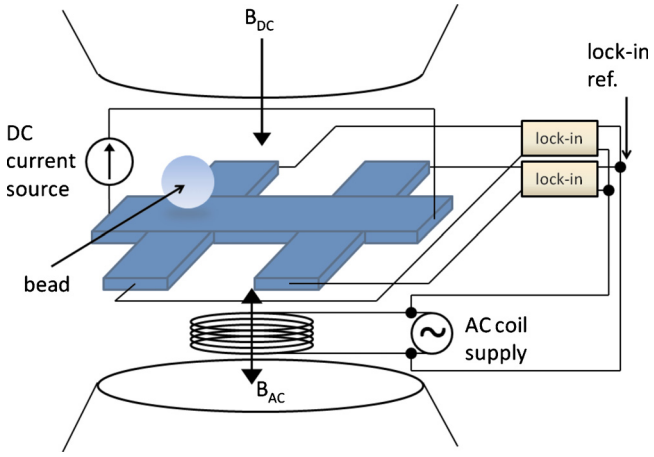

FIG. 1. (Color online) ac-dc voltage measurement setup. The picture is not in scale, the actual distance between the two crosses is ten times their width in order to avoid cross-talk between them.

bead was mounted on a Si membrane with a hole in the middle (Fig. 2), following the same procedure explained in Ref. 6.

The bias current was driven by a low-noise battery current source along the longitudinal lead while voltage across the transverse leads was simultaneously measured for both the crosses in dc as well as in ac measurements.

Where possible, twisted pairs were used in order to reduce inductive pick-up from the wiring and all the unnecessary metallic material was removed from the box and the near vicinity of the experimental setup.

Particle detection was carried out by applying ac and dc magnetic fields parallel to each other and perpendicular to cross surface[1,11,9] (Fig. 1). The ac field was produced by a coil ($L=5.87$ mH, $R=16.1\ \Omega$) driven by the ac voltage source with a peak-to-peak amplitude of 20 V. The chip-holder containing the devices was fixed to the coil by nylon screws and the whole setup was placed inside of a plastic

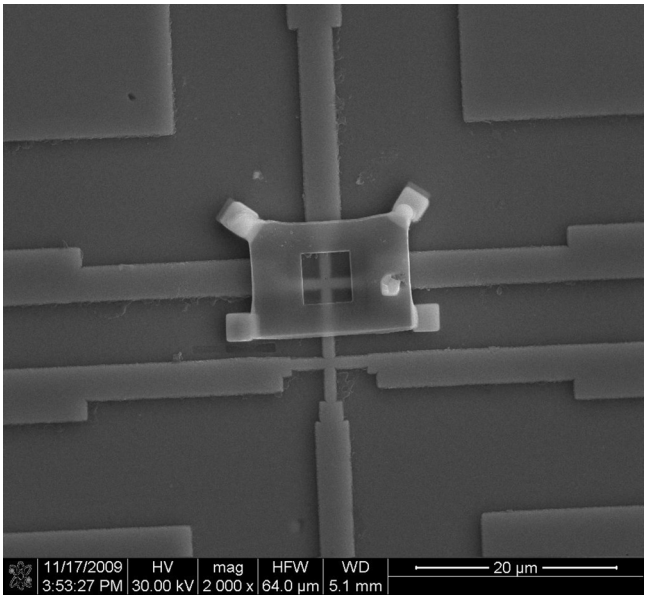

FIG. 2. SEM image of a double cross Hall sensor equipped with the Si membrane.

breakout box. At the position of the sensors the ac field amplitude was 9.2 mT peak-to-peak at low frequency. A drop was observed for $f>500$ Hz due to the coil capacitance. The dc field was produced by an electromagnet driven by a dc current source.

dc measurements were performed in order to characterize the Hall coefficients. Noise spectral density measurements were carried out by directly connecting a Stanford Research SR770 FFT spectrum analyzer to the voltage leads.

Two Stanford Research SR830 lock-in amplifiers were used for ac measurements, the reference signal was provided by the voltage drop across the ac coil, which has a constant phase shift of $\pi/2$ with respect to the ac field. A time constant of 3 s was used. The ac output of the crosses was measured both as a function of the dc field and as a function of time applying a step-wise dc field.

III. THEORY

The Hall voltage produced by a field B is given by

$$V_H = R_H I_{\text{bias}} B, \tag{1}$$

where R_H is the Hall coefficient and I_{bias} is the bias current. In typical experimental conditions B has three contributions:

$$B = B_{\text{ac}} + B_{\text{dc}} + B_{MM}, \tag{2}$$

where B_{dc} is the dc field,

$$B_{\text{ac}} = B_1(\omega) e^{i[\omega t + \phi(\omega)]} \tag{3}$$

is the ac field where both the amplitude B_1 and the phase ϕ are frequency dependent because of the coil resistance and capacitance, and $B_{MM}=CM(B)$ is the field due to the presence of any magnetic material with a magnetization M in the near vicinity of the crosses (C is a coupling constant). $M(B)$ could be expanded at the first order around B_{dc}:

$$M(B) \approx M(B_{\text{dc}}) + \chi(B_{\text{dc}}) B_{\text{ac}}, \tag{4}$$

where χ is the magnetic material susceptibility. In a real experimental setup B_{MM} is produced by both a superparamagnetic bead under study and the foreign magnetic material unavoidably present near the sensors, for example, in wiring or in the chip holder. It should be noted that, while all possible precautions to eliminate such spurious contributions were undertaken, the experimental measurements still detected the presence of uncontrollable magnetic material.

Using Eqs. (1) and (4), the ac Hall voltage V_H^{ac} is given by

$$V_H^{\text{ac}}(B_{\text{dc}}) = R_H I_{\text{bias}} [1 + C\chi(B_{\text{dc}})] B_{\text{ac}}. \tag{5}$$

An inductive parasitic signal is expected to be always detected, it can be written in the form

$$V_{ind}(\omega, B_{\text{dc}}) \approx \alpha(\omega, B_{\text{dc}}) \frac{dB}{dt}, \tag{6}$$

where the parameter α couples the voltage lead loops with the time-varying components of the field. In principle, this parameter can depend on both the frequency and the dc field. Using Eqs. (4) and (6), V_{ind} becomes

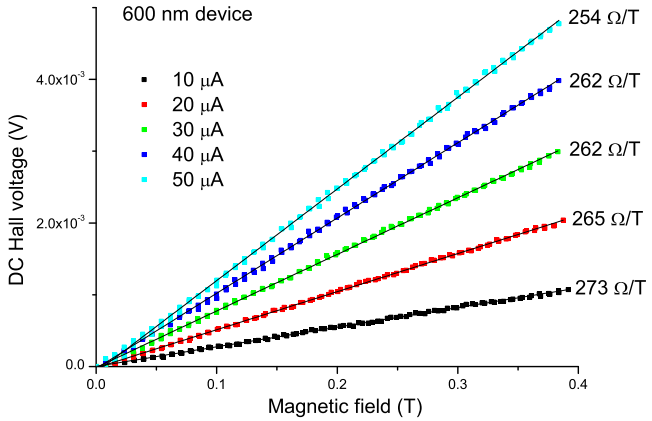

FIG. 3. (Color online) dc Hall voltage as a function of dc field for different bias currents, the solid lines are best linear fits. Hall coefficients are reported on the graph.

$$V_{ind}(\omega,B_{\rm dc}) = i\omega\alpha(\omega,B_{\rm dc}) \times [1 + C\chi(B_{\rm dc})]B_{\rm ac}. \quad (7)$$

The total measured ac signal is thus $V_{\rm tot}^{\rm ac} = V_H^{\rm ac} + V_{ind}$.

For the magnetic beads used in this work $\chi'' \ll \chi'$ at room temperature, where χ' and χ'' are the real and imaginary parts of χ, respectively. Thus, V_{tot} could be separated into amplitude (V_{tot}^{amp}) and phase (Ψ) components or in-phase (V_x) and out-of-phase (V_y) components with respect to $B_{\rm ac}$:

$$V_{tot}^{amp}(\omega,B_{\rm dc}) = [1 + C\chi(B_{\rm dc})]B_1(\omega) \times \sqrt{R_H^2 I_{\rm bias}^2 + \omega^2\alpha^2(\omega,B_{\rm dc})}, \quad (8)$$

$$\Psi(\omega,B_{\rm dc}) = \tan^{-1}\left(\frac{\omega\alpha(\omega,B_{\rm dc})}{R_H I_{\rm bias}}\right), \quad (9)$$

$$V_x(\omega,B_{\rm dc}) = R_H I_{\rm bias} \times [1 + C\chi(B_{\rm dc})]B_1(\omega), \quad (10)$$

$$V_y(\omega,B_{\rm dc}) = \omega\alpha(\omega,B_{\rm dc}) \times [1 + C\chi(B_{\rm dc})]B_1(\omega). \quad (11)$$

Equations (8) and (9) show that the measured ac voltage amplitude always contains both inductive and magnetic-material effects while the phase is only dependent on the inductive pick-up. Thus, Ψ is a good control parameter to check the reduction of parasitic inductive effects.

On the other hand, from Eqs. (10) and (11) one can derive that all the effects related to magnetic materials must be in-phase with $B_{\rm ac}$, while the out-of-phase component contains all the parasitic inductive effects.

IV. OPTIMIZATION OF MEASUREMENT PARAMETERS

In order to optimize the experimental setup configuration, several empty crosses with widths between 600 nm and 5 μm were fully characterized. The measured Hall coefficients were between 170 and 1180 Ω/T. Figure 3 demonstrates the Hall coefficient dependence on the bias current for the smallest device. Noise spectra showed a low-frequency $1/f$ behavior of the power spectral density, which increases with the bias current (Fig. 4). The white noise level was 32 $nV/Hz^{1/2}$ for a standard 600 nm device, this corresponds to a sensitivity of $B_{\rm min}=2.5$ $\mu T/Hz^{1/2}$ with a typical bias current of 50 μA. For optimized low-resistance devices,

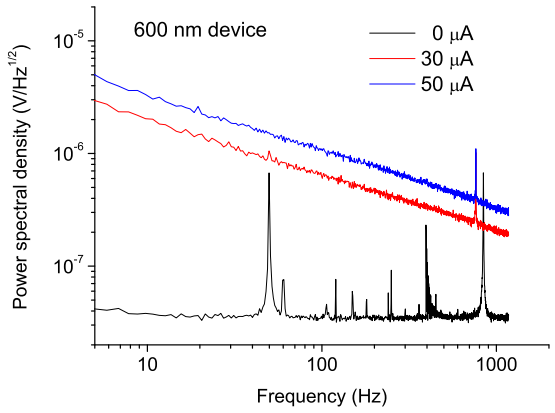

FIG. 4. (Color online) Noise power spectral density at different bias currents.

with long metallic leads, and a significantly higher $R_H = 1106$ Ω/T, a sensitivity of $B_{\rm min}=5.4$ $\mu T/Hz^{1/2}$ was achieved with a bias current of 5 μA.

In order to characterize the device response above the noise level, ac voltage measurements as a function of $B_{\rm dc}$ were taken averaging 30–50 times (Fig. 5). The signal amplitude plots always showed a hysteresis cycle, indicating the presence of ferromagnetic material of an unknown origin close to the sample. The phase signals did not show any significant hysteresis, being largely unaffected by magnetic materials, in agreement with Eq. (9). On the other hand, the quasi-linear drift in the phase can be ascribed to pure inductive effects.

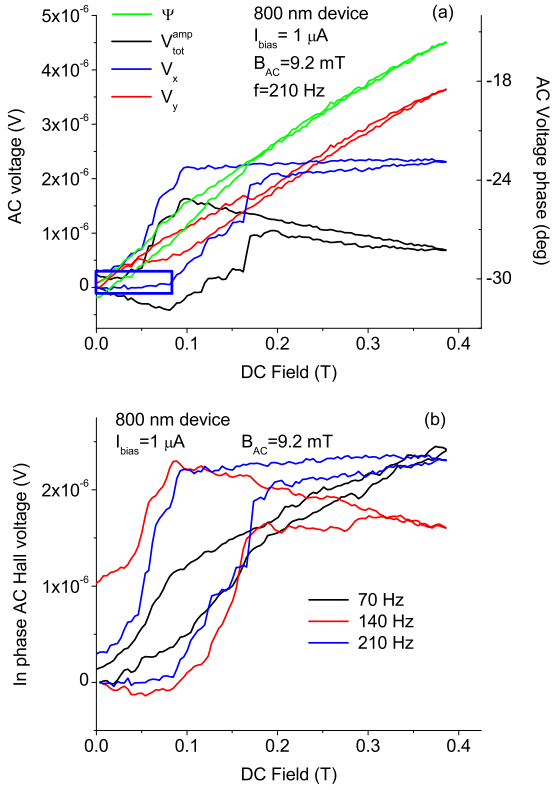

FIG. 5. (Color online) (a) ac voltage amplitude (V_{tot}^{amp}), phase (Ψ), in-phase component (V_x) and out-of-phase component (V_y) as a function of dc field for 800 nm wide InSb Hall bar at $f=210$ Hz. The blue box highlights the optimal dc field range for bead detection. (b) dc field dependence of V_x at different frequencies. $B_{\rm dc}$ has been swept between 0 and 0.388 T in both directions.

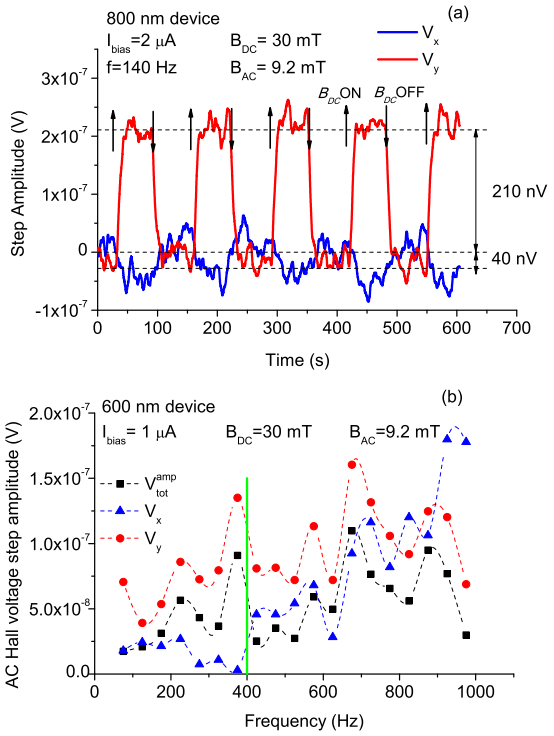

FIG. 6. (Color online) (a) In-phase (V_x) and out-of-phase (V_y) components of the ac voltage in response to B_{dc} steps between 0 and 0.03 T with a duration of 60 s (800 nm device). (b) Steps amplitude in V_x, V_y and total ac amplitude (V_{tot}^{amp}) as a function of the frequency (600 nm device). Dashed lines connecting experimental points are guides for the eye. The vertical line marks the area where $V_x \ll V_y$.

In agreement with Eq. (10), the parasitic hysteresis was always present in the in-phase ac voltage components (V_x) that, compared with the overall amplitude, also showed a smaller slope in the flat regions of the hysteresis cycle. This could be seen as an evidence that V_x was actually free from inductive effects being influenced only by magnetic materials. The out-of-phase components (V_y) evolved following the phase, but being also affected by magnetic material contributions [Eq. (11)], it showed a slightly larger hysteresis.

For all the measured devices a relatively flat part of the curves $V_x(B_{dc})$ has always been observed at low dc fields, this makes V_x suitable for bead detection when applying sufficiently small B_{dc} steps. Indeed, the inductive response has been observed in V_y, while the steps in V_x were just above the noise level [Fig. 6(a)].

This characteristic has been observed for frequencies up to 400 Hz, where the resulting step amplitude in V_x was always significantly smaller than that in V_y, and also in the total amplitude [Fig. 6(b)]. For larger frequencies this tendency was never preserved, most probably because of capacitive effects which cause the voltage signal across the coil to undergo a phase shift with respect to the actual B_{ac} phase. Thus, for $f > 400$ Hz, in-phase and out-of-phase components are no longer properly separated.

Taking into account the noise spectra and the high frequency phase shift in the lock-ins reference and B_{AC} amplitude drop, the optimal frequency range for bead detection experiments was determined to be in the range 140–270 Hz.

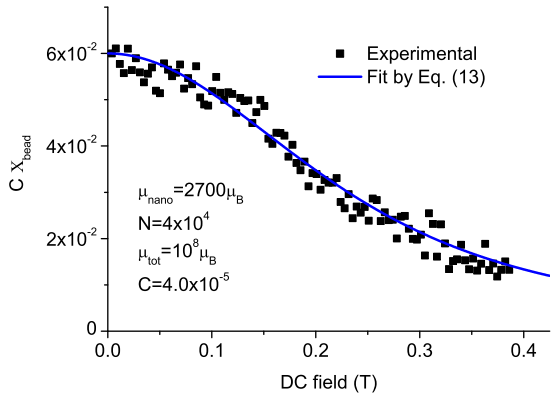

FIG. 7. (Color online) Experimental magnetic susceptibility of a single FePt nanobead (∅ 140 nm, $\mu \approx 10^8$ μ_B) scaled by bead-to-sensor coupling constant (■) and fitted by Eq. (13) (solid line).

V. BEAD DETECTION

Working with a 600 nm double cross, the detection of a single magnetic bead of 140 nm in diameter was achieved using the optimized experimental setup. The bead was composed of $N \approx 4 \times 10^4$ FePt nanoparticles ≈3–4 nm in diameter and was held around 200 nm above one of the crosses using the Si membrane (Fig. 2). The Hall coefficients of the crosses were $R_H^1 = 262$ and $R_H^2 = 174$ Ω/T at $I_{bias} = 30$ μA for crosses with and without the bead, respectively. The detection was carried out through the direct measurement of the susceptibility as a function of B_{dc} and was performed at the frequency of 270 Hz. Since the distance between the two crosses is around 6 μm one can assume that the artifact signal produced by ferromagnetic materials was the same on both the crosses, while the stray field from the bead was only detected by the nearest sensor. Thus, normalizing V_x signals by the Hall coefficients and dividing by the bias current and the ac field amplitude it turns out:

$$C\chi(B_{dc}) = \frac{1}{I_{bias}B_1}\left[\frac{V_x^{1(bead)}}{R_H^1} - \frac{V_x^{2(no\ bead)}}{R_H^2}\right]. \quad (12)$$

As the first approximation, the magnetization of a superparamagnetic bead, above the critical temperature, could be expressed by Langevin function and, correspondingly, its susceptibility is obtained by differentiation with respect to magnetic field:

$$\chi \approx \frac{N\mu_{nano}}{k_BT}\left[\left(\frac{k_BT}{\mu_{nano}B_{dc}}\right)^2 - \frac{1}{\sinh^2\left(\frac{\mu_{nano}B_{dc}}{k_BT}\right)}\right], \quad (13)$$

where μ_{nano} is the magnetic moment of a single FePt nanoparticle. By fitting the experimental $\chi(B_{dc})$ curve with the function in Eq. (13) (Fig. 7), the following parameters were estimated: $\mu_{nano} \approx 2700$ μ_B for an individual 3–4 nm FePt nanoparticle and $\mu \approx 10^8$ μ_B for the whole FePt bead. The corresponding coupling constant was $C \approx 4 \times 10^{-5}$. Potentially the sensitivity of this detection method could be significantly improved by increasing the bead-cross coupling.[11] This could be achieved using smaller crosses and/or decreasing the distance between the bead and the sensor active layer. In our case, the presence of the Si membrane, necessary to

protect the semiconductor during the positioning operations, forces a lower limit to this parameter. The development of a non destructive manipulation technique able to position the bead in direct contact with the semiconductor and the fabrication of narrower crosses could allow the detection of much smaller magnetic moments.

It is necessary to underline that the procedure described by Eq. (12) cannot be applied without the elimination of inductive signals, i.e., using V_{tot}^{amp} instead of V_x. Due to variations in the geometry of voltage leads, the inductive pick-up signals are generally different for the two crosses and cannot be simply excluded by subtracting the ac voltage data.

VI. CONCLUSIONS

Because of the small magnetic moments involved, the detection of nanometric magnetic beads employing high-sensitivity Hall measurements requires careful examination of the experimental setup. The optimized ac-dc phase-sensitive detection method presented here allows separation of both inductive pick up signals and foreign magnetic material effects from the real signal produced by the bead under measurement. Taking as a reference the ac field phase, the successful separation of inductive signals in the out-of-phase component of ac voltage has been observed experimentally and explained with simple calculations. After the optimization of measurement frequency and the complete characterization of a large number of InSb double crosses with varying geometry, size and resistance, the detection of a single FePt bead with a diameter of 140 nm and a magnetic moment of $\approx 10^8$ μ_B has been performed, using a 600 nm-wide device, through the direct measurement of its magnetic susceptibility. This careful characterization approach is essential if spurious signals are to be eliminated. We believe our method is capable of future refinement, to improve still further the bead detection sensitivity.

ACKNOWLEDGMENTS

This work has been funded by the UK BIS under Project No. 114503 and EU FP7 NanoSpin (T4.J02). We are grateful to P. See and D. Cox for their technical inputs, L. Cohen for providing InSb films and useful discussions and M. Spasova for providing FePt nanoparticles.

[1] G. Mihajlović, P. Xiong, S. von Molnár, K. Othani, H. Ohno, M. Field, and G. J. Sullivan, Appl. Phys. Lett. **87**, 112502 (2005).
[2] P. Manandhar, K. Chen, K. Aledealat, G. Mihajlović, C. S. Yun, M. Field, G. J. Sullivan, G. F. Strouse, P. B. Chase, S. von Molnár, and P. Xiong, Nanotechnology **20**, 355501 (2009).
[3] K. Togawa, H. Sanbonsugi, A. Sandhu, M. Abe, K. N. H. Narimatsu, and H. Handa, J. Appl. Phys. **99**, 08P103 (2006).
[4] K. Togawa, H. Sanbonsugi, A. Sandhu, M. Abe, H. Narimatsu, K. Nishio, and H. Handa, Jpn. J. Appl. Phys., Part 2 **44**, L1494 (2005).
[5] G. Mihajlović, P. Xiong, S. von Molnár, M. Field, and G. J. Sullivan, J. Appl. Phys. **102**, 034506 (2007).
[6] O. Kazakova, V. Panchal, J. Gallop, P. See, D. C. Cox, M. Spasova, and L. F. Cohen, J. Appl. Phys. **107**, 09E708 (2010).
[7] W. Lee, S. Joo, S. U. Kim, K. Rhie, J. Hong, K.-H. Shin, and K. H. Kim, Appl. Phys. Lett. **94**, 153903 (2009).
[8] A. Sandhu, H. Sanbonsugi, I. Shibasaki, M. Abe, and H. Handa, Jpn. J. Appl. Phys. **43**, 777 (2004).
[9] P. Besse, G. Boero, M. Demierre, V. Pott, and R. Popovic, Appl. Phys. Lett. **80**, 4199 (2002).
[10] A. Kerlain and V. Mosser, Sens. Actuators, A **142**, 528 (2008).
[11] G. Mihajlović, K. Aledealat, P. Xiong, S. von Molnár, M. Field, and G. J. Sullivan, J. Appl. Phys. **97**, 172518 (2007).